Proc. of XXX Summer School "Advanced Problems in Mechanics"
St.-Petersburg, Russia, 2003, June 27 - July 6, c. 230-239

Computer Simulation of Mechanical Properties for Powder Particles Using Molecular Dynamics

F. A. Gilabert A. M. Krivtsov A. Castellanos

gilav@us.es

Abstract

A computational model for polymer particles used in xerographic and printing industries is presented. The powder grain is modelled by a cluster containing thousands of particles interacting via an empirical potential. The grain is subjected to various mechanical tests. The objective is to select the appropriate potential of interaction and the internal structure for the computer material for the adequate simulation of the mechanical behaviour of the real toner grains.

1 Introduction

A special interesting topic in the physics of fine granular material or most commonly called fine powders, is the problem of adhesion, as it is well known that interparticle forces have a very important effect in the nature of the contact [1]. Previous to any proposition for a molecular dynamics model for adhesion between two powder grains, it is important first to characterize their mechanical properties. In the particular case of our computational investigation we will have in mind the material used in our real experiments with powder, a copolymer called Polystyrene-Butadiene. Its mechanical properties have been measured from physical experiments of compression [2], and exactly the same task has been reproduced and imitated numerically. The main aim of this work is the mechanical characterization of the computer material by means of different ways of compression. Firstly, a specimen is generated using an aggregate of spheres which are joined by the action of a fitness empirical potential. Secondly, by increasing the number of particles per unit of volume, we determine the minimum number required to characterize the mechanical properties. Depending on the size of the material grain, our description may be mesoscopic or microscopic. In the former case, the spheres (the basic units of the computer material) are not real atoms, but elements of a higher scale level. For grains small enough, the number of particles can be the same as the number of real atoms, in which case we will refer to these units as atoms, and our description is truly microscopic. Then, an ensemble made of many particles interacting by a prescribed potential can represent our model of the material grain. We work with two types of structures, both of them with different theoretical and well-determined mechanical properties. This is necessary to check the validity of our results. Once the model is validated, we modify the shape and range of the potential searching for the desired mechanical behaviour, since the set of the theoretical relations that link the internal parameters of the potential with the macroscopic mechanical magnitude have been obtained only in the closest neighbor approximation.

2 Creation of the specimens

To generate the initial configurations, we have considered a simple procedure to obtain amorphous and FCC[1] specimens. For generation of the amorphous specimens we start with a SC[2] structure composed of many particles, the interaction is switched on at the beginning of the simulation, integrating the equations of motion for a system of N particles interacting via a potential $\Pi(r)$. This structure is geometrically unstable. To promote the instability the initial perturbation is made by adding a randomized component to the particle velocities. As a result the inner structure of the specimen is rearranged to an amorphus structure — Figure 1. To generate the stable FCC structure we have used as initial configuration a slightly perturbated FCC structure, to originate from here the stable configuration, as in Figure 1. When we say “stable” we mean that the final result is a specimen with a very low mean kinetic energy. To achieve this equilibrium configuration we add a viscous term to the equations of motion, in order to dissipate kinetic energy as the system evolves on time. Hence the equations of motion for the particles are

$$m\frac{d^2\vec{r}_i}{dt^2} = -\sum_{j=1}^{n_i} \nabla_j \Pi(r_{ij}) - B\vec{v}_i \,, \tag{1}$$

where m is the mass of the particle, B is the coefficient of viscosity, $r_{ij} \stackrel{\text{def}}{=} |\vec{r}_i - \vec{r}_j|$, the sum is over all those neighbors of the particle i whose positions are within the cutoff distance of the potential. We are solving these equations of motion using a centered scheme in finite differences. To speed up the calculations, a method of primitive mesh and divisions in computational cells has been used, where interactions between particles are constrained just for neighbor cells, avoiding in this way loops of N^2 interactions.

[1] Face-Centered Cubic
[2] Simple Cubic

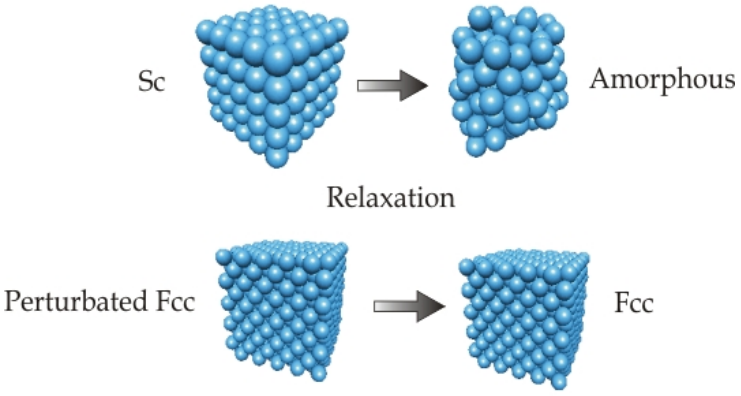

Figure 1: Creating Amorphous and FCC configurations.

A variety of potentials have been tried. We have started our simulations using the LJ (Lennard-Jones) potential, which has frequently been used to simulate Argon crystals [3]

$$\Pi(r_{ij}) = D\left[\left(\frac{a}{r_{ij}}\right)^{12} - 2\left(\frac{a}{r_{ij}}\right)^{6}\right]. \tag{2}$$

In the following, the Morse potential has also been considered

$$\Pi(r_{ij}) = D\left[e^{-2\alpha(r_{ij}-a)} - 2e^{-\alpha(r_{ij}-a)}\right]. \tag{3}$$

In this notation, D is the depth of the well and a is the equilibrium distance between two particles interacting by the potential. Several values for the non-dimensional parameter $\rho \stackrel{\text{def}}{=} a\alpha$ has been considered in the range of 6–16 to note the differences with the LJ potential. Further extensions of this range can be done if necessary.

Regarding the computational units, the unit of time has been the period of oscillation of a single particle of mass m

$$T_0 \stackrel{\text{def}}{=} 2\pi\sqrt{\frac{m}{C}}, \tag{4}$$

where C is the stiffness of the bond and it can be defined as the second derivative of the potential evaluated at the distance of equilibrium, a

$$C \stackrel{\text{def}}{=} \Pi''(a). \tag{5}$$

The unit for the velocity has been the dissociation velocity

$$v_d \stackrel{\text{def}}{=} \frac{\pi}{3}\frac{a}{T_0}. \tag{6}$$

This is the necessary velocity for the particle to reach the infinity from its position of equilibrium in the potential field $\Pi(r)$. The coefficient of viscosity is measured in the terms of its critical value $B_0 \stackrel{\text{def}}{=} 2\sqrt{mC}$. In this work, we have set the viscous coefficient as 3% of B_0.

3 Experiments of uniaxial compression

Once the specimen has been generated, it was subjected to a number of compression test. In this work, we have used the following four methods: static uniform deformation, constant volume force, constant deformation rate using rigid walls, periodic boundary conditions method. For FCC crystals all the compression tests were performed along the $[1, 0, 0]$ direction of the crystal.

3.1 Applying a static uniform deformation

To verify the dynamics simulations a static test on uniform deformation was considered. The specimen is uniformly deformed as a result of moving each particle from its stable position to its new displaced one. We have considered not more then 0.1% deformation to be under the conditions of the linear theory of elasticity. Then the stresses in the material were measured, which allow calculating the elastic moduli. Note that no time integration was used during this test.

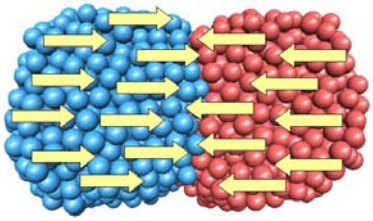

Figure 2: Compression of two grains by applying a constant volume force.

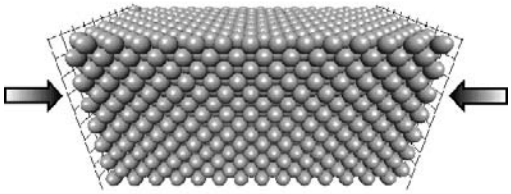

Figure 3: Compression of FCC specimen by compressive walls.

3.2 Applying a constant volume force

The preparation of this computational experiment consists in placing together two blocks made of the computer material, as it is shown in Figure 2. A compressive stress in the area of contact will be imposed by means of the application of a constant force on each particle. Let σ be the compressive stress that the specimen should reach in equilibrium. This stress is the result of the ratio between the total force F that one grain exerts on another and the area of contact S. The area of contact S will change when the force is acting, therefore we need a technique as accurate as possible to measure the area of contact, since this surface is rough and irregular. This was estimated with enough accurateness using detection of the particles, which belonged to this area. The force that should be applied on each particle is

$$F_{\text{atom}} = \frac{F}{N}\,, \tag{7}$$

where F is the total force acting on the specimen and N the number of the particles in the specimen. On the other hand, it is convenient to express the numerical magnitudes in a non-dimensional form, then we will consider the following unit for the stress

$$\sigma_0 \stackrel{\text{def}}{=} \frac{f_{\text{max}}}{a^2}\,, \tag{8}$$

and we can express

$$\sigma = K_\sigma \sigma_0\,, \tag{9}$$

where f_{max} is the necessary strength to break the bond when only two particles are interacting, a is the distance of equilibrium and K_σ is the intensity of the stress. Combining the above definitions, one obtains the following relation

$$F_{\text{atom}} = \frac{K_\sigma \sigma_0 S}{N}\,. \tag{10}$$

In this kind of experiment we need to reach an equilibrated compressive state with a final concrete value for the stress between the grains (σ, or K_σ in the units of σ_0) which allows us to obtain the elastic moduli for the computer material. Let us note that the same problem which allows an analytical determination of the Young modulus [4] can be obtained considering a body being compressed by its own weight.

3.3 Applying a constant deformation rate using rigid walls

In this section, we have carried out the compression experiment using a simulated press. This press consists of two rigid walls that can be moved one towards another at a constant velocity. Our computational material will be compressed between the two walls. We can impose the deformation rate for the specimen just controlling the velocity of the walls. The friction between the specimen and the walls is neglected. This way of compression is specifically convenient when a FCC specimen is being studied, because it can have a tight contact with the wall. Some additional precautions must be undertaken for amorphous specimens, since their geometrical surfaces are irregular. In most of the cases the wall can compress just some points belonging to the specimen, and then some local changes may modify the surface structure, for example, inducing order, and even local crystallization. In this experiment, the stress in the area of contact between both cubical grains is measured. Special attention has been paid to the measuring the area of contact, because for small specimens we can have ambiguity in the values of the Young modulus and Poisson ratio due to the fact that there are several ways to measure the size of the contact area. However, the larger is the specimen the more negligible is this effect [5].

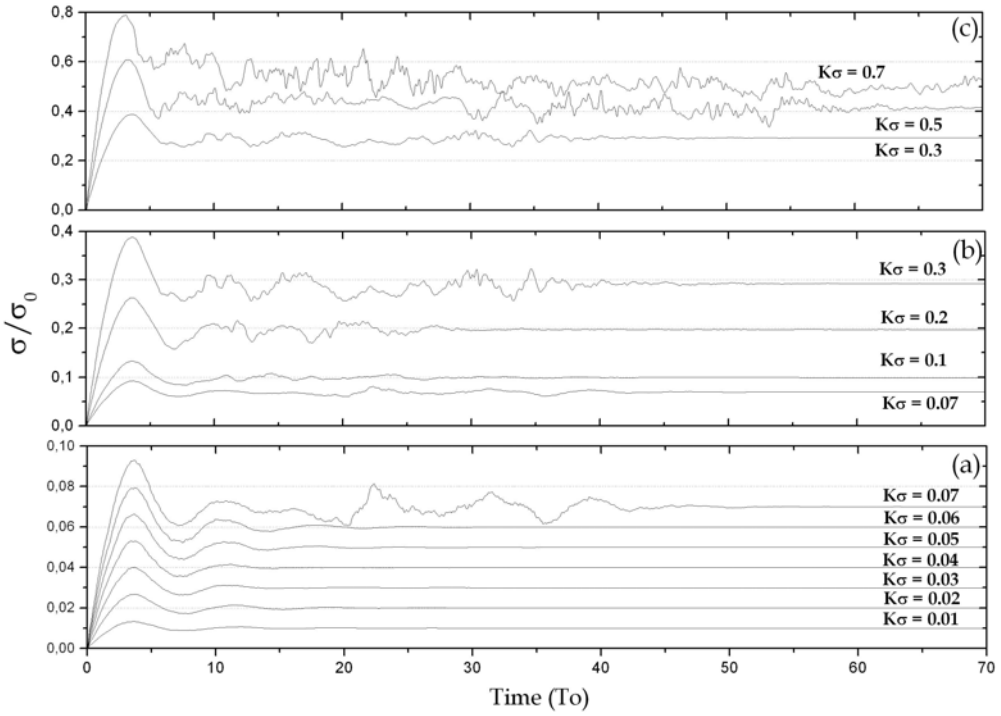

Figure 4: (a) Elastic deformation, (b)plastic deformation and (c) breakage. The volume force experiments using a LJ amorphous specimen.

3.4 Periodic boundary conditions method

In this method periodic boundary conditions are applied in the three spatial directions. To perform the test initially a uniform uniaxial deformation ε_x is applied in the same way as in the static test. The same deformation is applied to the periodic cell. Then the time integration of the equations of motion is performed during the time interval T_0, and for $t > T_0$ the integration is continued until the deviation of the velocities decrease below the critical value: $\Delta v < 0.1|\varepsilon_x|$, which depends on the considered deformation ε_x.

After the time integration is finished the normal stresses σ_x, σ_y, σ_z are measured in the specimen. Then the following formulae are used for determining the components of the stiffness tensor

$$C_{xx} \stackrel{\text{def}}{=} (\sigma_x - \sigma_x^0)/\varepsilon_x\,, \qquad C_{yx} \stackrel{\text{def}}{=} (\sigma_y - \sigma_y^0)/\varepsilon_x\,, \qquad C_{zx} \stackrel{\text{def}}{=} (\sigma_z - \sigma_z^0)/\varepsilon_x\,, \tag{11}$$

where σ_x^0, σ_y^0, σ_z^0 are the stresses in the initial configuration. According to the technology of the specimen creation this stresses should be very small, nevertheless they should be taken into account for the precise determination of the elastic moduli. Next, the obtained stiffness coefficients are used to determine the Young modulus E and Poisson ratio ν of the material

$$E \stackrel{\text{def}}{=} C_{xx} - 2\nu C_{yz}\,, \qquad \nu \stackrel{\text{def}}{=} \frac{C_{yz}}{C_{yz} + C_{xx}}\,, \qquad C_{yz} \stackrel{\text{def}}{=} \frac{C_{yx} + C_{zx}}{2}\,. \tag{12}$$

Since the material should be isotropic, the values for the moduli C_{yx}, C_{zx}, C_{yz} obtained from the above formulae should be generally equal. However, due to the finite size of the specimens some deviations from the isotropy can be noticed. That is why the averaging formula for the coefficient C_{yz} is used above to decrease the possible errors.

4 Mechanical behaviour

In this section we present some results for different types of specimens using various potentials. In the case of constant volume force, we were considering amorphous specimens with potentials LJ and Morse 10. For the test with compressive walls, some results with FCC structures using LJ, Morse 6 and Morse 10 potentials are presented.

The parameter αa from the Morse potential is connected to the brittleness of the interaction. It is known that if the value $\rho = \alpha a \simeq 6$ for the Morse potential is considered, a very similar shape to the LJ potential will be obtained. However for different values of ρ there are clear differences that can guide us to select the appropriate shape for the potential. We begin commenting the numerical results of uniaxial volume load using an amorphous specimen created with a LJ potential. It must be noted that the load is not really quasistatical, and therefore a time of relaxation must be observed to obtain a state of equilibrium. The reason for presenting all mechanical magnitudes versus time is that this is a dynamic process. As we can see in the graphs of Figure 4, three different behaviors can be observed. Each of them corresponds to the stress (in units of σ_0) versus time. Each curve corresponds

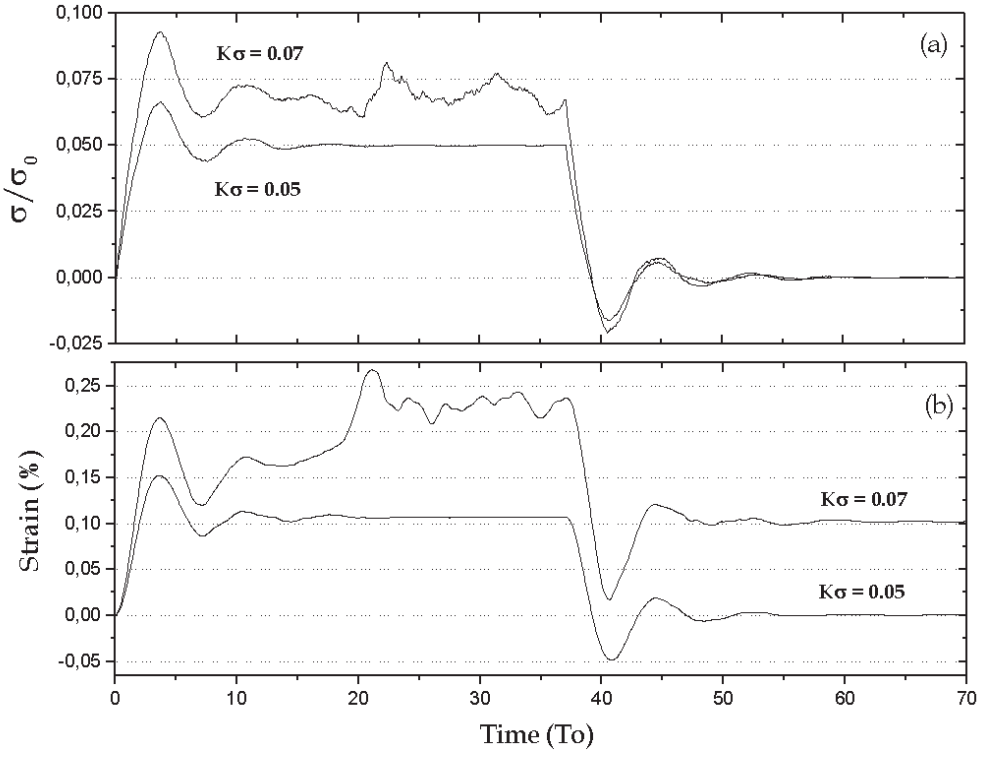

c

Figure 5: Elastic and plastic recovering of a LJ amorphous specimen in a volume force experiments. It can be seen that the fluctuation in the stress are correlated with the residual deformation.

to an intensity of stress in the area of contact. In Figure 4a, a state of equilibrium has been reached for the imposed stress. In this state, the deformation will be completely reversible if the elastic limit is not surpassed, as it can be seen in Figure 5 for the case $K_\sigma = 0.05$ as example. This means that if the force is removed (Figure 5a), the specimen recovers its initial state. However, if a value of stress is equal or slightly larger than the yield strength, then fluctuations appear at the stress curve (Figures 4 and Figure 5a with $K_\sigma > 0.06$), indicating that a fraction of the energy given to the system has been dissipated to heat. Therefore, a residual deformation exists, as we can see in Figure 5b. It can also be noted that a plastic flow has been produced when the material reaches a new internal state. This is more evident when a larger value of the stress is imposed. When the material is in the plastic state, the equilibrium can be reached, but the achieved stresses are always less than the imposed original values (Figure 4b). However, if a higher value of stress is imposed, an equilibrium will never be reached (Figure 4c), since once the ultimate strength is surpassed the material will break and it will flow permanently.

When exactly the same experiment is carried out with a specimen subjected to a Morse 10 potential, some differences were observed (Figure 6). From Figure 6a one can observe that the plastic field is not as clear as before. It seems that the material can reach the breakage point directly from the elastic zone. It is a classical feature of the brittle material like some glasses or ceramics. Once the ultimate strength in compression is reached, this material breaks and its initial internal structure becomes irretrievable. In graph ν versus time (Figure 6c) a good agreement can be seen with the theoretical value of amorphous specimens, which is about 0.25. However for the LJ specimens this value in equilibrium is about 0.36 (Figure 7). A possible reason for this small deviation is that the considered theoretical values have been calculated taking into account the closest neighbor approximation. It works correctly with the Morse 10 potential since it is of shorter range than the LJ potential. In our simulations we have considered a cutoff distance equal to $2.1a$, evidently taking into account a greater number of spheres than the closest neighbor approximation. The Young modulus has been computed using a considerable number of tests. Figure 8 shows the results of the uniaxial compression test of an amorphous specimen compressed by walls. This graph exhibits the typical features of a glassy polymer. In the beginning it shows a linear response, then it is followed by a region of plastic flow where the maximum values of the stresses are limited. For the polystyrene one finds that the strain corresponding to the yield stress is within the interval between 1.1% and 2.5%, while strain at maximum stress is between 4% and 6%. Of course, these are features for non-treated polystyrene, it means that it can found that for filled or reinforced polystyrene these features can vary. In fact, for the polymers is well-known that their mechanical response depend strongly on the velocity of deformation. In our case, a low velocity of deformation compared with the dissociation velocity has been considered. We have compared this behaviour with physical experiments [6], and we have found a good agreement with values for the elastic and ultimate yield strength. On the other hand, the numerical values for the elastic moduli compared with the theoretical predictions we have not found such a good agreement, concretely for the amorphous specimens. It must be noted that in this case the internal degrees of freedom have to be taken into account. These degrees of freedom are neglected in the static tests because we impose the exact motion and therefore these results are closer to the theoretical calculations where averaging of the

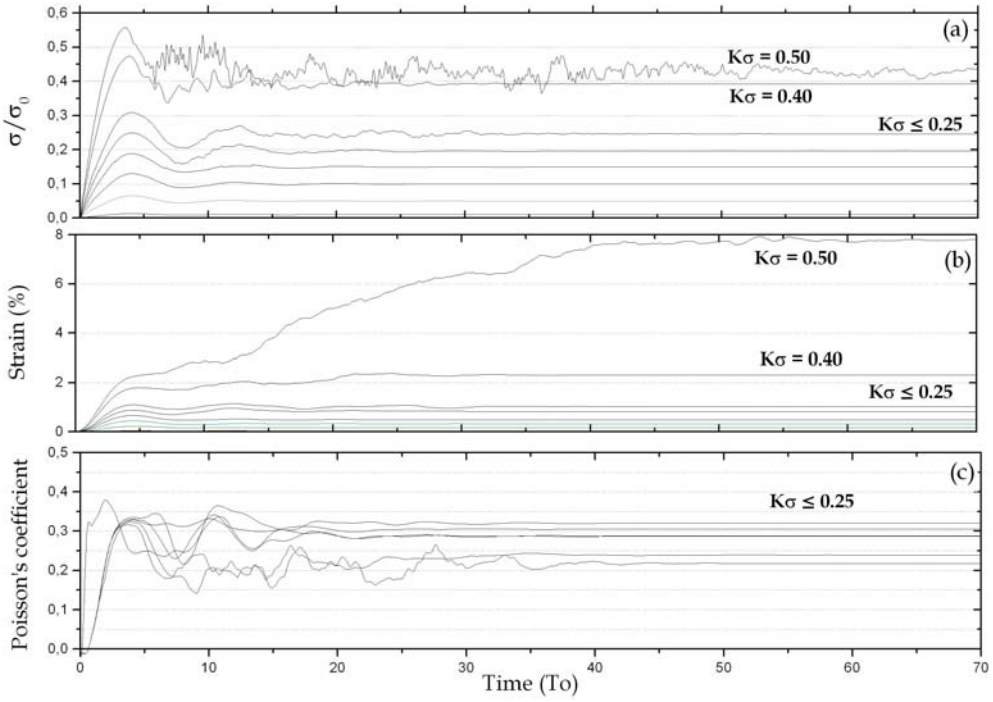

Figure 6: (a) Stress-time, (b) strain-time and (c) Poisson ratio-time for Morse 10 specimen, volume force method.

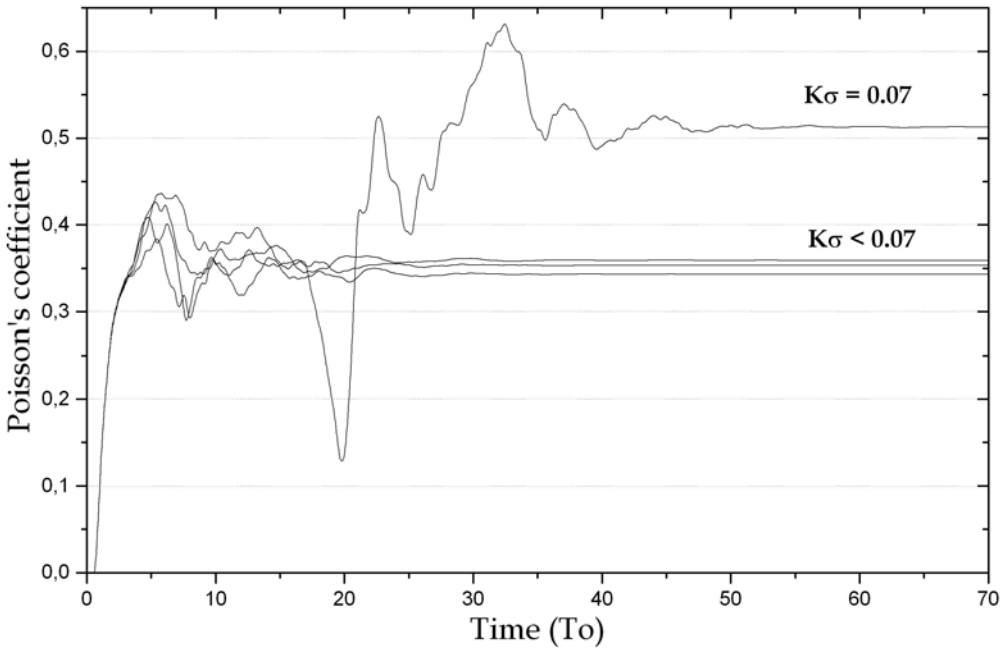

Figure 7: Poisson ratio versus time for LJ amorphous specimen in the volume force experiment.

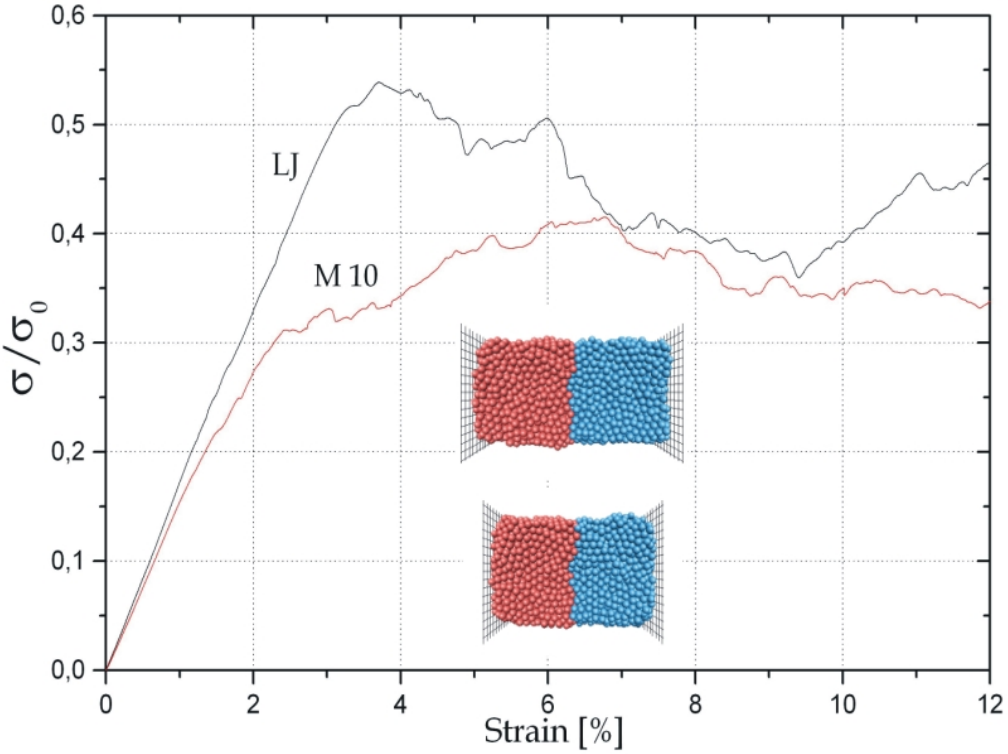

Figure 8: Stress-strain diagram of a specimen made of 6750 particles. It can be seen that LJ specimen shows similar behaviour to a fairly brittle polymer. The result for the Morse 10 specimen is not so clear.

elastic moduli in all directions is performed. Therefore, the most reliable results are obtained from the dynamics calculations, where these internal degrees are included. On the other hand, some additional errors are playing an important role in our results, as we mentioned previously, in relation to the size of our specimens.

During the uniaxial compression of FCC structures using a pair of rigid walls, for several specimens, we have noted an structural change in the specimens. The resulting graphs and the three dimensional visualization, suggest that this structural change could be related to a phase transition from the FCC to HCP[3] lattice. This is closely connected with the phenomenon of martensitic phase transition [7], usually obtained by a very fast cooling and getting a new and more compact atomic rearrangement. The physics of these phase transitions is not well-known yet in spite of the fact that they have a wide range of applications, e.g. to increase the hardness of steels. Studies of this phenomenon using Molecular Dynamics could be a promising direction of investigation.

To simulate a quasistatical compression a very low deformation rate has been imposed. For this part of this work, we have set the velocity of deformation to be a small fraction of v_d, concretely $5 \cdot 10^{-3} v_d$. As Figure 9 shows, the result is a typical stress-strain diagram known for many real materials. We have placed numbers in this graph for the Morse 10 specimen, corresponding to the snapshots in Figure 10. In Figure 9, it can be seen that the material created using Morse 10 potential is the brittlest, with the absence of the plastic field. It should be noted that phase transitions occur for each specimen, although in Morse 10 it is more evident and faster. This is because in the Morse 10 specimen bonds have a shorter range, and the phase transition takes place rapidly after the shear is originated on the sliding plane [1,1,1] of the crystal. However, for LJ and Morse 6 specimens, this breakage of the bonds is more gradual. At the plastic zone, a non-reversible rearrangement takes place that leads to the beginning of the phase transition. As one can see in Figure 9, the stage marked as 5, a slope reappears: now, walls are compressing a HCP structure. If after the second breakage the walls continue compressing the specimen, a new breakage will be obtained with the structure of the material already destroyed; the third pick of the stress is precisely the compression of this disordered structure.

5 Elastic moduli determination

Comparing the results of the elastic moduli determination obtained from the different tests we deduced that the best accuracy is reached using the PBC (Periodic boundary conditions) method. In other methods the errors due to the finite size of the specimens are relatively high and only very big specimens (containing more then 10^5 particles) can give acceptable accuracy.

In Table 1 the results of Young modulus determination using PBC method for the LJ amorphous specimens are shown. To compare with the theoretical calculations the cutoff distance in Table 1 is set to $1.3a$, which relates to the close neighbor approximation.

[3]Hexagonal Close-Packed

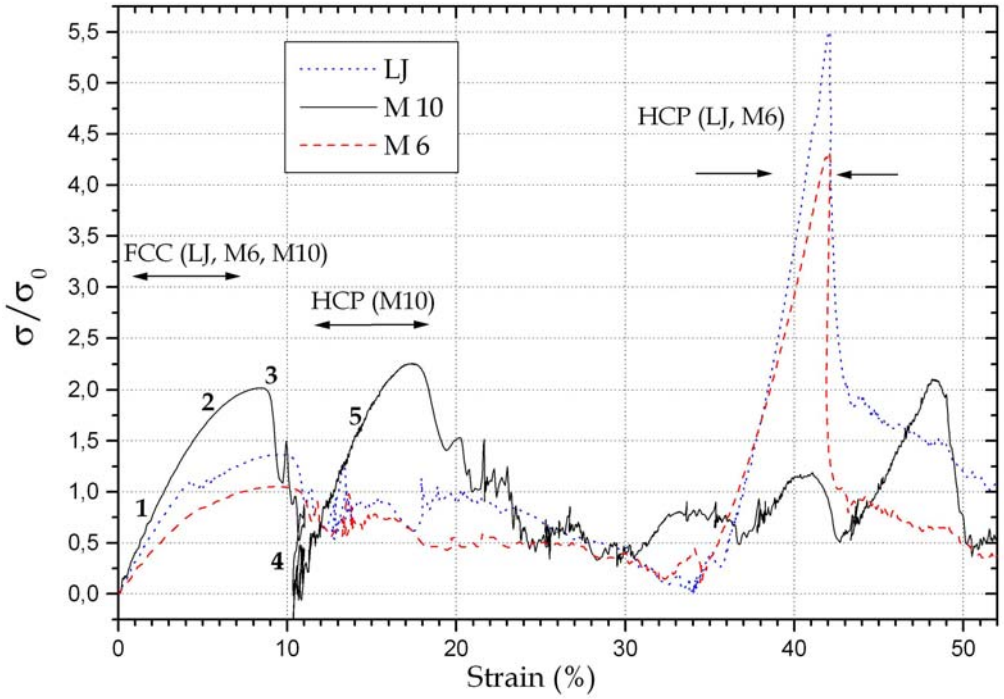

Figure 9: Stress-strain diagram for FCC specimens.

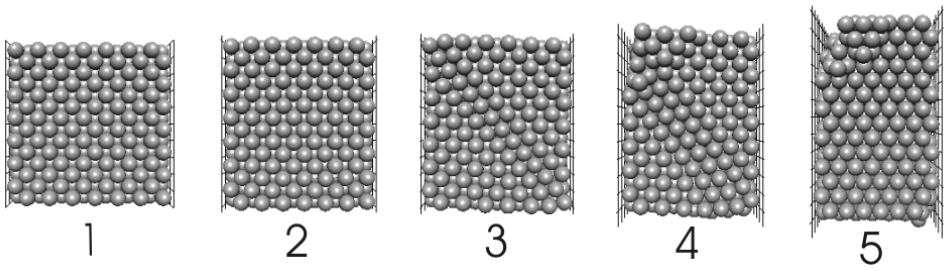

Figure 10: Snapshots of the phase transition from FCC to HCP structure.

	FCC	Amorphous	Amorphous
Number of particles	Any	1000	8000
E/σ_0, theoretical	25.2360	37.8540	37.8540
E/σ_0, static	25.2360	34.2 ± 0.6	33.9 ± 0.2
E/σ_0, equilibrium	25.2360	20.4 ± 0.7	20.0 ± 0.2

Table 1: Results of the Young modulus determination for the LJ amorphous specimens in the close neighbor approximation.

The theoretical values for the Young modulus of FCC and amorphous structures are calculated using the following formulae

$$E_{\text{FCC}} = \frac{2\sqrt{2}}{3}\,\frac{C}{a}\,, \qquad E_{\text{am}} = \sqrt{2}\,\frac{C}{a}\,; \qquad \sigma_0 = \frac{7}{169}\,\sqrt[6]{\frac{7}{13}}\,\frac{C}{a}\,, \tag{13}$$

where the representations for the Young moduli are valid for any pair interaction, while the formula for σ_0 is true for the LJ interaction only. The above formula for E_{FCC} corresponds to $[1,0,0]$ direction of the crystal, the formula for E_{am} is obtained by averaging the stiffness tensor of the FCC crystal over all space directions [8].

The static value for the Young modulus in Table 1 is obtained immediately after setting the uniform deformation, before the time integration starts. The equilibrium values are obtained via time integration until all the particles reach their equilibrium positions (e.g. the velocity deviation will be below its critical value: $\Delta v < 0.1|\varepsilon_x|$).

For the FCC crystal the test deformation was $\varepsilon_x = \pm 10^{-8}$, which allows obtaining 6 correct digits[4]. For the amorphous specimens the test deformation was $\varepsilon_x = 10^{-4}$, which is sufficient to eliminate the nonlinear effects for the desired accuracy. The numerical results for the amorphous specimens are obtained from the set of ten experiments, from which the average value and the standard deviation are obtained.

As it follows from Table 1, for the FCC crystal all the considered methods give exactly the same results. For the amorphous specimens the situation is different. From the table it can be seen that the theoretical values and the static method values are more or less close to each other, but the equilibrium values are quite different. The explanation of this inconsistency is that the internal degrees of freedom in the amorphous specimen are neglected in both theoretical and static methods, and this gives much higher values for the stiffnesses that the correct values, obtained after the system reaches the equilibrium.

Analysis of the results, obtained by increasing the number of particles from 1000 to 8000 (see Table 1) shows that the standard deviation became smaller, but the average values does not change much, which proves that the scale effect is almost negligible and further increase in the number of particles is not necessary.

The results of the elastic moduli determination using PBC method for the LJ specimens with the cutoff distance $2.1a$ is shown in Table 2. This cutoff distance is the working distance for all other calculations in this paper. This distance is big enough so that the interaction with the further neighbors can be neglected. For the FCC specimens both static and equilibrium moduli are equal, but for the amorphous specimens only true (equilibrium) moduli are shown in the table.

	FCC	Amorphous
Young modulus, E/σ_0	30.1692	22.5 ± 0.8
Poisson ratio, ν	0.357907	0.377 ± 0.004

Table 2: Elastic moduli for the LJ specimens with the cutoff distance $2.1a$.

6 Conclusions

Table 3 shows comparison of the typical mechanical properties of polystyrene in comparison with the same mechanical properties of the amorphous computer material with the LJ interaction[5]. Only the dimensional parameters, such as the strength ratio σ_u/E

Quantity	Symbol	Polystyrene	Computer material	Computer material
Density	ρ	1065 kg/m^3	$1.009\,\rho_0$	1065 kg/m^3
Young modulus	E	3.0 GPa	$22.5\,\sigma_0$	3.6 GPa
Ultimate strength	σ_u	90 MPa	$0.50\,\sigma_0$	80 MPa
Strength ratio	σ_u/E	3.0 %	2.2 %	2.2 %
Poisson ratio	ν	0.33	0.38	0.38

Table 3: Mechanical properties of polystyrene and the selected computer material.

and the Poisson ratio ν can be compared directly. To compare the dimensional properties the computational parameters ρ_0 and σ_0

[4] To increase the accuracy the average of the results from the compression and tension tests was calculated.

[5] The values of ultimate strength correspond to compression tests.

in the Table 3 should be set. Choosing $\rho_0 = 1056$ kg/m^3 and $\sigma_0 = 160$ MPa gives the properties for the considered computer material, which are shown in the last column of Table 3. This gives exact agreement for the density value and moderate agreement for the elastic and strength properties, which is acceptable due to significant variation in the known experimental data. Using Morse potential, in principle, it is possible to obtain exactly the considered elastic and strength properties by varying the additional parameter of the potential. But this is not essential, since the experimental values are not accurate, and there is no sense in obtaining exact accuracy. Besides, the LJ potential is more convenient for the numerical realization and also is more understandable from the physical point of view, since it is proved to describe well the Van der Waals interactions. Given that the inner structure of the polystyrene is amorphous, we consider an amorphous ensemble of particles as the most appropriate internal structure for the computational material. The stress-strain diagram exhibited in Figure 8 for the amorphous specimen using the LJ potential shows a good agreement with the real compression tests using specimens of polystyrene. Thus, using an amorphous ensemble of particles interacting via the LJ potential achieves the computer material with the mechanical properties, which are acceptable to model mechanical behaviour of the polystyrene powder particles.

Acknowledgements

This research was supported by Spanish Government Agency Ministerio de Ciencia y Tecnología (DGES) under Contract No. BFM2000-1056, NATO Collaborative Linkage Grant PST.CLG.976575, and RFBR grant No. 02-01-00514.

References

[1] Ed. D. S. Rimai, L. P DeMejo and K. L. Mittal. Fundamentals of Adhesion and Intefaces. VSP, Utrecht, The Netherlands, 1995.

[2] D. Pann. Private communication.

[3] A. Rahman, Phys. Rev. A, No 136, 1964, p. 405.

[4] S. Timoshenko. Theory of the elasticity. McGraw-Hill, New York, 1970.

[5] A. M. Krivtsov and N. F. Morozov. Dokl. Phys., Vol. 46, No 11, 2001, pp. 825–827.

[6] R. Quinson, J. Perez, M. Rink and A. Pavan. J. Mat. Sci. No 32, 1997, pp. 1371–1379.

[7] A. G. Khachaturyan, Theory of Structural Transformations in Solids. Wiley, New York, 1983.

[8] A. M. Krivtsov. Isotropic part of nonlinear constitutive equations of ideal crystal lattice. J. of St. Petersburg State Techn. Univ. ("Trudy SPbGTU"), Vol. 458, 1995, pp. 132–140 (in Russian).

F. A. Gilabert, Seville, Spain

A. M. Krivtsov, St. Petersburg, Russia

A. Castellanos, Seville, Spain